Thinking in 360°: Humanoid Visual Search in the Wild

Heyang Yu^{1*} Yinan Han^{3*} Xiangyu Zhang⁴ Baiqiao Yin¹ Bowen Chang¹ Xiangyu Han¹ Xinhao Liu¹ Jing Zhang¹ Marco Pavone^{2,5} Chen Feng^{1†} Saining Xie^{1†} Yiming Li^{1,2†}

¹NYU ²NVIDIA ³TU Darmstadt ⁴UC Berkeley ⁵Stanford University

https://humanoid-vstar.github.io

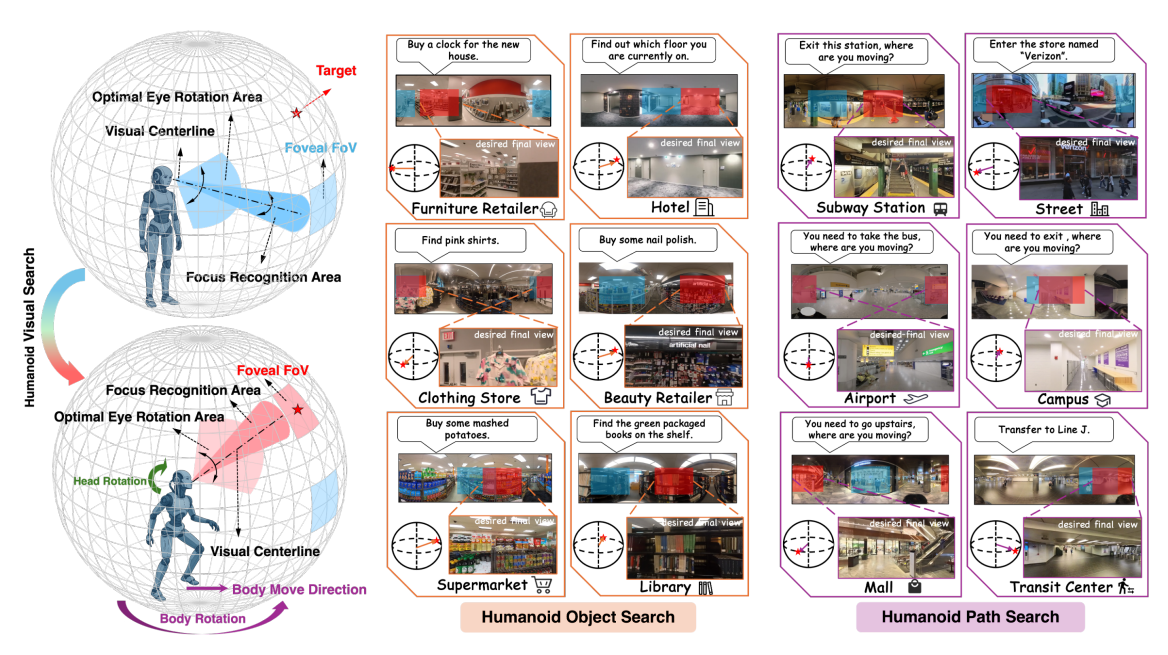


Figure 1. We pose a fundamental question: can an AI agent actively search for objects or paths in a 3D world like a human, rather than just passively describe what it sees? We transition agents from passive captioners to active searchers, moving them from constrained household scenes into the rich complexity of the wild. A key enabler is our scalable paradigm where a single 360° panorama closes the perception-action loop for head rotation, freeing active embodied reasoning in real life from hardware constraints.

Abstract

Humans rely on the synergistic control of head (cephalomotor) and eye (oculomotor) to efficiently search for visual information in 360°. However, prior approaches to visual search are limited to a static image, neglecting the physical embodiment and its interaction with the 3D world. How can we develop embodied visual search agents as efficient as humans while bypassing the constraints imposed by realworld hardware? To this end, we propose humanoid visual search where a humanoid agent actively rotates its head to search for objects or paths in an immersive world represented by a 360° panoramic image. To study visual search in visually-crowded real-world scenarios, we build

 H^*Bench , a new benchmark that moves beyond household scenes to challenging in-the-wild scenes that necessitate advanced visual-spatial reasoning capabilities, such as transportation hubs, large-scale retail spaces, urban streets, and public institutions. Our experiments first reveal that even top-tier proprietary models falter, achieving only ~30% success in object and path search. We then use post-training techniques to enhance the open-source Qwen2.5-VL, increasing its success rate by over threefold for both object search (14.83% \rightarrow 47.38%) and path search (6.44% \rightarrow 24.94%). Notably, the lower ceiling of path search reveals its inherent difficulty, which we attribute to the demand for sophisticated spatial commonsense. Our results not only show a promising path forward but also quantify the immense challenge that remains in building MLLM agents that can be seamlessly integrated into everyday human life.

^{*}Equal contribution.

[†]Equal advising.

1. Introduction

The human visual system is highly efficient, capturing sharp detail only at the fovea while leaving other regions blurred or unseen [39]. Despite the sensor limitations, humans efficiently perform visual search tasks in 360° (*e.g.*, locating the next exit in a crowded subway station) by rapidly executing saccades and deliberately reorienting their head, minimizing sensory redundancy and computational cost.

Recent state-of-the-art computational methods for visual search are based on Multimodal Large Language Models (MLLMs), leveraging their rich world knowledge to enhance the generalization capability. These methods commonly process a single, static, low-resolution image. Subsequent actions are typically confined to computational operations (e.g., cropping and zooming within this fixed canvas) to enhance resolution and glean detail [38, 58, 66]. However, these methods suffer from two fundamental gaps compared to biological visual search [5]: (1) Non-interactive: Lacking an interactive simulator, the model cannot change its perspective to obtain information beyond its initial field of view. (2) Disembodied: Lacking physical embodiment, the model cannot couple visual reasoning with actions in the physical world. Moreover, the search is usually not driven by embodied tasks (e.g., manipulation or navigation), reducing it to an abstract perceptual exercise rather than a real-world, goal-directed behavior [32, 51, 67]. In other words, developing an embodied visual agent that can actively search for information in visually crowded scenes remains underexplored, despite its significant potential in humanoid robots, assistive technology, and augmented reality.

To bridge these gaps, we prototype humanoid visual search (HVS), where humanoid agents couple deliberate reasoning with active head turns for visual search in complex environments. Specifically, (1) HVS is interactive. The agent starts with a narrow perspective view but acts within a lightweight 360° panorama, enabling a closedloop perception-action cycle in which each head rotation changes its visual input. (2) HVS is embodied. It tightly couples visual reasoning with physical action, requiring agents to deliberately coordinate head movements as part of their thought process. Meanwhile, the search is driven by embodied tasks, defined in two core forms: a. humanoid object search (HOS): Locating and foveating a target object as a prerequisite for manipulation. b. humanoid path search (HPS): Identifying a navigable path to a destination and aligning body orientation as a prerequisite for locomotion. To systematically study *HVS*, we raise the question:

What environments truly necessitate advanced visual-spatial reasoning capabilities?

We argue that human-made environments rich in *structural* (multi-level layouts), *semantic* (dense compositional cues), and *volumetric* (cluttered 3D space) complexities offer the

most valuable testbed for such reasoning. We therefore *shift* our focus beyond simplistic constrained scenarios such as household object search toward in-the-wild challenges, such as: navigating the multi-level labyrinth of a subway station to find a specific exit, identifying a particular store in a large shopping mall, or retrieving a specific product from a densely stocked supermarket aisle. Unfortunately, existing embodied AI platforms often suffer from limited perceptual realism [6, 16, 59] or are restricted to household scenes [15, 31, 47, 60], failing to represent the rich, dense, and cluttered environments that necessitate advanced visual-spatial reasoning capabilities.

To this end, we introduce H^*Bench , a new benchmark featuring diverse in-the-wild scenes suitable for HVS, including but not limited to transportation hubs (airports and subway stations), large-scale retail spaces (supermarkets and shopping malls), and public institutions (libraries and museums), as shown in Fig. 1. Each panoramic image is densely annotated with embodied task questions and corresponding ground-truth actions: optimal head orientations for HOS and unit direction vectors on the ground plane for HPS. We evaluate MLLMs in their ability to focus on taskdriven visual details and generate embodied plans in diverse human environments. Our experiments show that supervised fine-tuning (SFT) and reinforcement learning (RL) can enhance performance, yet also reveal major unresolved challenges, highlighting the long-term value of research in this domain. Our contributions are listed as follows.

- We introduce humanoid visual search, a **novel task** enabling human-like active spatial reasoning in 360°.
- We propose a scalable framework that leverages realworld 360° panoramas as lightweight simulators, creating a hardware-free platform to study embodied reasoning.
- We build *H*Bench*, the first **systematic benchmark** of its kind, with dense annotations on panoramic scenes from challenging in-the-wild environments.
- We conduct **thorough evaluations** to show that posttraining can improve the performance of MLLMs, while also highlighting promising avenues for future work.

2. Related Works

Visual Search. As a hallmark of *System 2* slow thinking [25], visual search involves deliberate reasoning to identify objects or information within visually crowded environments. Early visual search methods use bottom-up visual saliency, top-down contextual guidance, or a combination of both [40, 56, 65]. Yet these studies often fail to generalize due to their limitations in contextual understanding. Recent advances in visual search, pioneered by V^* [58], are driven by MLLMs with rich world knowledge (e.g., object co-occurrence) to achieve better performance. However, existing work focuses on search within static 2D images, without considering the active and embodied nature of visual

search in the 3D world. Prior neuroscience studies reveal that human visual search coordinates eyes and head in a nested system, in which the head preferentially explores unseen regions, while the eyes exploit already-visible content via finer-scale saccades [4, 30, 50]. We prototype a visual search model with human-like eye-head coordination.

Visual Navigation. Visual navigation, along with visionlanguage navigation, aims to develop agents that can move through an environment to reach a specified goal [2, 72]. The core of these tasks lies in completing the entire trajectory as fast as possible. However, this requires a 3D simulator or real hardware: realistic simulators are hard to build, and real-world experiments are difficult to scale and reproduce. As a result, previous efforts are mostly limited to household scenes where 3D data is easier to acquire [7–10, 37, 45, 71], leaving in-the-wild challenges underexplored. Our work is motivated by the observation that human reasoning is intermittent during navigation; it is invoked only at critical decision points. Focusing on these critical points enables us to build a closed-loop search environment directly from in-the-wild 360° panoramas, bypassing the need for 3D simulation or physical hardware and yielding a scalable framework for embodied visual search. In summary, we focus on active, embodied, and multimodal reasoning in visually crowded 360° scenes, a key prerequisite for open-world navigation and mobile manipulation.

Multimodal LLMs. Multimodal LLMs can understand and reason about multiple modalities of information (e.g., text and images), representing a promising pathway toward Artificial General Intelligence (AGI). Seminar works focus on effectively aligning the feature spaces of pretrained visual encoders with those of LLMs, including Flamingo [1], BLIP [33, 34], and LLaVA [35]. Recently, Tong et al. [55] conduct a systematic vision-centric exploration and propose a token-efficient connector to integrate high-resolution vision features with LLMs. Meanwhile, a new wave of MLLMs, such as GPT-40 [41] and Gemini 2.5 [46], has set new state-of-the-art benchmarks across multimodal tasks by scaling model capacity and introducing novel training recipes. One crucial technique is reinforcement learning (RL)-based post-training, which further aligns model outputs with human preferences, enhances instruction-following capabilities, and mitigates hallucination and bias [43, 63]. RL can also incentivize strong reasoning abilities when coupled with verifiable rewards, particularly for complex tasks such as mathematical problem solving and multistep logical reasoning [20, 22, 27, 28]. We ground MLLMs in the physical world to assess and improve their performance in active and embodied visual search.

Multimodal LLMs with Tools. Just as humans leverage external tools to transcend their innate physical and cognitive limitations, a similar paradigm is now empowering artificial intelligence. Recently, LLM agents demonstrate

superior performance in solving challenging long-horizon tasks [24, 42], a capability unlocked by providing them with an external toolkit (e.g., web browsing, code execution) and refining their policies through multi-turn reinforcement learning [17, 18]. This approach is now being extended to multimodal settings, where MLLMs generate a symbolic tool call (e.g., OCR, marking, cropping, zoom in) at each reasoning step to overcome its limitations in semantic grounding and visual perception [36, 44, 49, 67, 70]. Among these tools, iterative zoom-in and region-of-interest selection are particularly well-suited for visual search tasks, enabling active perception over images. However, these operations still occur on a disembodied 2D canvas, where the tool (action) is confined to computational manipulations of a static image file. We couple the use of the tool with the actions in the physical world: active head rotation is called to continuously construct a visual chain of thought. This bridges the critical gap between passive visual reasoning and active embodied reasoning.

Multimodal LLMs for Embodied Reasoning. While LLMs trained on Internet data may acquire rich world knowledge, they struggle to ground that knowledge in the physical world due to the large gap between symbolic linguistic representations and embodied perception. To bridge the gap, a growing body of research aims to ground MLLMs in embodied reasoning [12, 23, 54, 64, 68]. To build more general models, Cosmos-Reason1 [3] enables MLLMs to perceive the physical world through video input and reason about it to generate more physically grounded responses, including explanatory insights and embodied decisions. Gemini Robotics-ER [52] extends Gemini's multimodal reasoning capabilities to the physical world, with enhanced spatiotemporal understanding. Yet active visual search with interleaved multimodal reasoning remains unexplored.

3. Humanoid Visual Search

Human spatial intelligence is punctuated by critical decision points where we stop to observe, reason, and resolve ambiguity before acting with confidence. Our task focuses on these critical points, abstracting full-body motion into the *atomic action* of head rotation. This is motivated by the crucial role of cephalomotor control in human visual search, allowing us to study the core cognitive processes of embodied visual search in a tractable yet realistic manner.

3.1. Problem Formulation

Objective. Imagine a humanoid agent equipped with a limited field-of-view (FoV) navigating a complex, multi-corridor junction in a subway station, tasked with locating an exit as quickly as possible. The limited FoV necessitates a tight coordination between head and eye movements: the head explores the unknown by rotating to new vantage points, while the eyes exploit the already-seen information

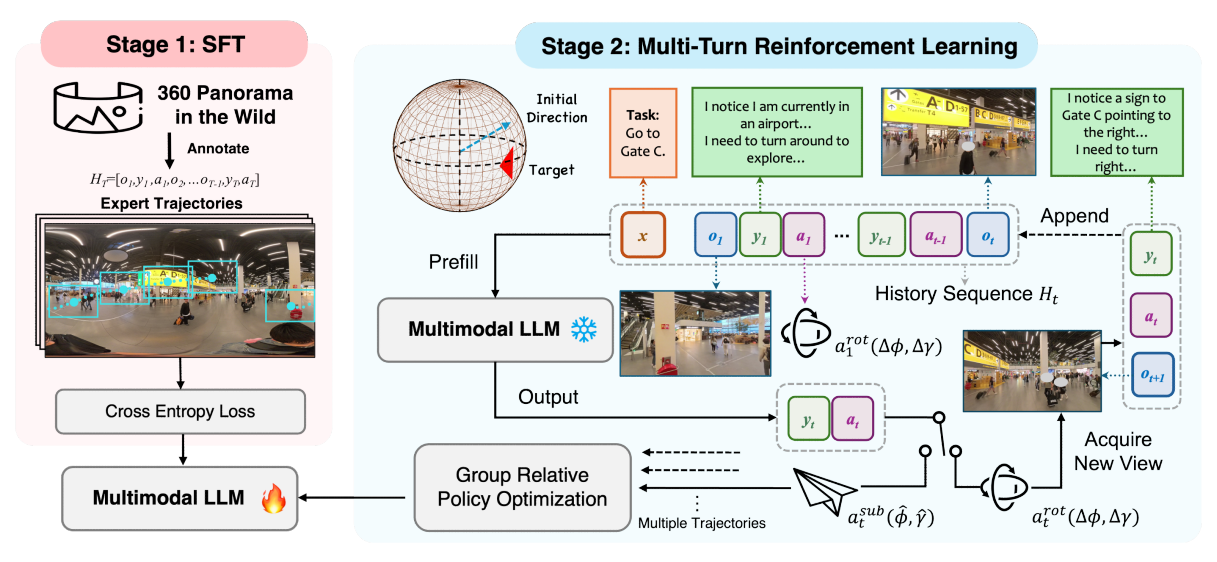


Figure 2. **Pipeline Illustration.** Stage 1 (SFT) provides the foundational ability to map perspective images to plausible actions (e.g., turning around upon seeing nothing). Stage 2 (RL) refines this into a strategic policy: the model learns to explore (outputting a_t^{rot}) until it acquires a view with sufficient evidence (e.g., spotting the gate sign), at which point it confidently submits the final estimate (a_t^{sub}).

by fixating on task-relevant details. Formally, we model the environment as a single 360° panoramic image. The set of all possible observations, $S_o = \{o_{\phi,\gamma}\}$, comprises narrow-FoV perspective images sampled from this panorama, each defined by its azimuth (ϕ) and polar angle (γ) . The goal of HVS is to identify the optimal direction (ϕ^*, γ^*) that maximizes the probability of task success r_s given the language instruction x and visual observation $o_{\phi,\gamma}$:

$$(\phi^*, \gamma^*) = \arg\max_{\phi, \gamma} P(r_s \mid o_{\phi, \gamma}, x).$$

Humanoid Object Search (HOS). HOS tackles the problem of active target search in an unknown 3D environment by finding a final viewing direction (ϕ^*, γ^*) that brings the target into the central foveal region of the perspective view. **Humanoid Path Search (HPS).** HPS requires the agent to search for a navigable path to a target location as a high-level planning step before locomotion. The goal is to identify a final viewing direction ϕ^* that is aligned with the path.

3.2. Humanoid Visual Search with MLLMs

We frame humanoid visual search as a multimodal reasoning task by coupling MLLM tool use with head rotation. This is realized through a tool-augmented MLLM [21], with the agent policy defined as $\pi_{\theta}(y_t, a_t \mid o_t, x, \mathcal{H}_t)$. Specifically, at each timestep t, the agent generates a textual chain of thought y_t and an action a_t , conditioned on current observation $o_t = o_{\phi_t, \gamma_t}$, language instruction x and history states $\mathcal{H}_t = \{(o_i, y_i, a_i)\}_{i=1}^{t-1}$. Each search episode allows for a sequence of rotation actions, concluding with a submission action that yields the final output. The action space thus consists of two primitives:

- Rotate $a_t^{rot}=(\Delta\phi,\Delta\gamma)$: Adjusts the viewing direction, updating $\phi_{t+1}=\phi_t+\Delta\phi$ and $\gamma_{t+1}=\gamma_t+\Delta\gamma$ (right/up are positive; yaw is circular).
- **Submit** a_t^{sub} : Commits the current viewing direction as the final estimate $(\hat{\phi}, \hat{\gamma})$ and terminates the episode.

3.3. MLLM Post-Training

Trained on static, disembodied Internet data, MLLMs inherently lack the spatial commonsense and active 3D planning capabilities required for humanoid visual search. Our evaluations (Sec. 5.2) reveal that even state-of-the-art proprietary models like GPT-4o [41] achieve only $\sim\!20\%$ success. Hence, we adapt MLLMs into effective visual search agents through the two-stage post-training pipeline shown in Fig. 2. We outline the stages below while deferring detailed mathematical formulations to Appendix Sec. IV.

Stage 1: Supervised Fine-Tuning (SFT). We first perform SFT on a curated multi-turn dataset (Sec. 4.2) to instill basic task-orientied reasoning and tool-use abilities. This teaches the model to generate structured action plans from multi-modal inputs, establishing a strong behavioral prior.

Stage 2: Multi-Turn Reinforcement Learning (RL). We then refine the policy using Group Relative Policy Optimization (GRPO) [48]. This RL stage encourages long-horizon reasoning and is crucial for developing robust, generalizable search strategies beyond the imitation learning baseline according to the previous findings [14].

4. H*Bench

4.1. Dataset Overview

We introduce H^*Bench to systematically evaluate humanoid visual search in rich, dense, and visually cluttered

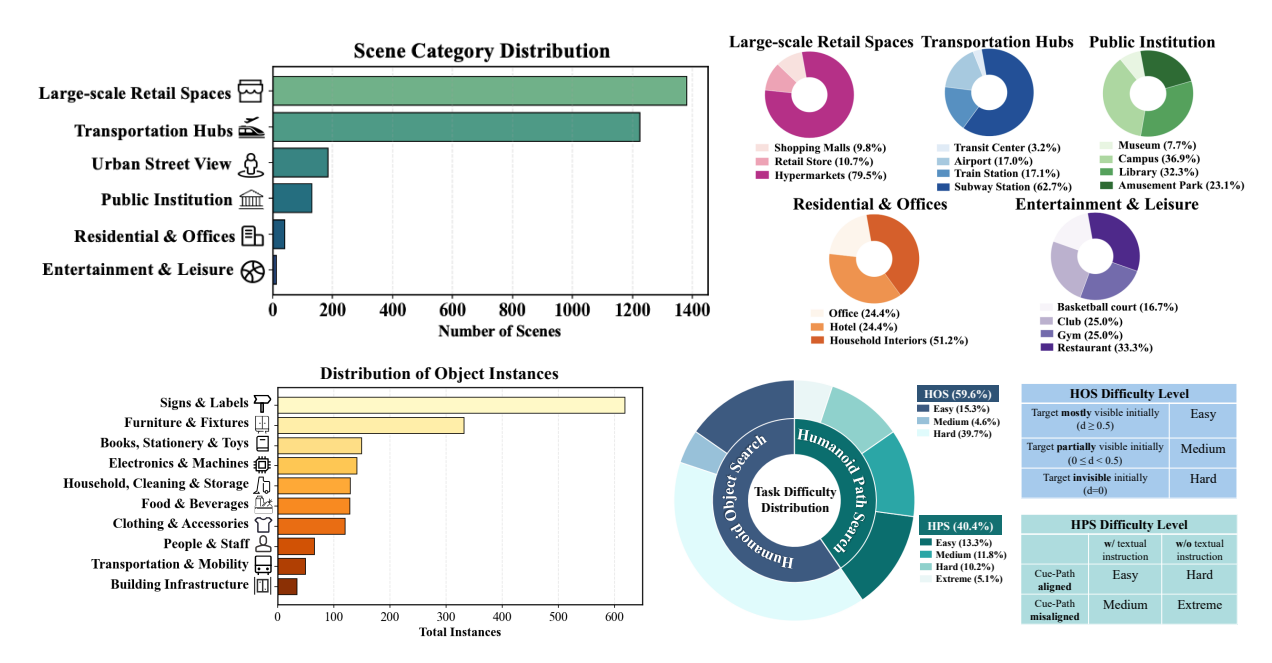


Figure 3. **Top Left:** Distribution of scene categories. **Top Right:** Sub-category composition per category. **Bottom Left:** Category-wise object instance distribution for *HOS*. **Bottom Right:** Task difficulty distribution and definition for *HOS* and *HPS*.

real-world environments. The benchmark comprises approximately 3,000 annotated task instances derived from a diverse set of high-resolution panoramic videos (up to 7680×3840). By initializing the agent with four distinct starting orientations per task instance, we obtain a total of 12,000 search episodes. Sourced from both self-collected footage across global metropolitan areas (New York, Paris, Amsterdam, Frankfurt) and open platforms (YouTube and the 360+x dataset [11]), **H***Bench delivers broad geographical coverage (see Appendix Sec. I) and substantial scene diversity (Fig. 3 Top). More specifically, it spans a wide spectrum of challenging scenarios across 12 countries, systematically organized into 6 major scene categories and 18 fine-grained scene types. These range from densely stocked retail environments and bustling transportation hubs to diverse public institutions and urban streets. Additionally, the diversity of *HOS* target objects is summarized in Fig. 3 Bottom Left. This breath across scenes and targets provides a rigorous and comprehensive evaluation testbed for assessing the visual search abilities of humanoid agents operating in complex real-world environments.

4.2. Benchmark Construction

Task Annotation. We annotate each panoramic scene in a perspective-view interface that renders narrow–field-of-view (FOV) images from the panorama at known viewing angles (ϕ, γ) . Annotators freely rotate the virtual camera to inspect the scene, identify a suitable embodied search task, write a natural-language instruction, and mark the target by drawing a tight bounding box that specifies its optimal di-

rection. The bounding box is then back-projected onto the panorama, and its center yields the optimal target direction (ϕ^*, γ^*) . For *HPS*, we retain only (ϕ^*) as the environment can be well approximated by a planar ground geometry.

Cold-Start Data Curation. To construct high-quality multi-turn trajectories for SFT, we select a subset of annotated task instances and augment them with structured chain-of-thought (CoT) rationales by prompting a strong MLLM (GPT-40 [41]). For each annotation step, given the task instruction, current observation, and the humanprovided optimal action (rotation angle or submit), GPT-40 is prompted to produce a concise, observation-grounded rationale explaining why the action is appropriate in context. We employ a human-in-the-loop protocol in which annotators review, and refine the generated rationales to eliminate hallucinations, ensure grounding in visible scene evidence, and enforce stylistic consistency. The resulting dataset consists of 2,000 multi-turn trajectories containing visual observations, verified CoT rationales, and actions, which we use to bootstrap SFT. In total, six annotators dedicated 250 hours to embodied question annotation and CoT refinement.

Difficulty Taxonomy. For HOS, we define task difficulty based on the initial visibility of the target object. We calculate a visibility ratio d as the fraction of the object area visible in the initial viewpoint compared to the complete area of the object. Higher visibility offers stronger perceptual cues and reduces exploratory burden, whereas lower visibility demands visual exploration during search. We therefore categorize HOS samples into Easy, Medium, and Hard (see Fig. 3 Bottom Right; visualizations in Fig. III). For

Table 1. **Left:** Quantitative results of open-source, proprietary, and fine-tuned models on H^*Bench . Top-three performances are highlighted with red, green and blue. **Right:** Performance comparison of the best-in-class open-source, proprietary, and fine-tuned models.

	Humanoid Object Search						Humanoid Path Search			HOS Overall	
Method	Overall	Easy	Medium	Hard	Overall	Easy	Medium	Hard	Extreme	HPS 47.38% HOS	
Open-Weight Multi Image Models										Extreme 47.38% Easy	
InternVL3.5-4B [13]	3.08	7.32	2.84	1.49	4.81	6.00	5.70	4.67	0.46		
InternVL3.5-8B [13]	6.38	9.76	9.10	4.79	7.25	10.00	7.68	5.14	4.17		
Qwen2.5-VL-3B-Instruct [61]	14.83	27.97	13.07	10.01	6.44	7.00	8.77	4.91	3.24	HPS Hard 25 75% HO Medi	
Qwen2.5-VL-7B-Instruct [61]	11.38	23.42	9.10	7.02	6.31	9.00	5.92	5.84	1.85	Hard 35.75% Medi	
Gemma-3-4B-it [19]	17.13	32.85	26.14	10.13	14.44	17.20	14.47	14.72	7.41		
Gemma-3-12B-it [19]	10.21	24.72	17.33	3.88	14.50	16.80	14.25	14.49	9.72	29.39%	
Kimi-VL-A3B-Instruct [53]	4.92	12.85	0.57	2.36	4.32	8.79	3.32	2.21	4.17		
Proprietary Models										HPS Medium 33,00% Hard	
GPT-4o [41]	19.75	18.17	17.35	20.92	23.69	26.80	22.59	26.17	13.89	41.60%	
Gemini2.5-Pro [46]	31.96	33.58	23.78	32.13	33.00	41.60	29.39	35.75	15.28		
Fine-Tuned Models (Ours)										HPS Easy HPS Overall	
HVS-3B (w/ SFT only)	40.83	53.82	23.86	37.73	23.00	28.00	23.03	21.26	14.81	Gemini2.5-Pro HOS Task	
HVS-3B	47.38	60.49	24.43	44.87	24.94	34.80	20.18	25.00	12.04	Gemma-3-4B-it HPS Task	
800000 Reg Reg (%) 477.4 477.1 29.5 288 200 14.8 29.5 28	56.8 60.		30.7 30.7 31.1	4	Cross-Task (SFT + R HVS-3B 45.3 44.9 33.4	ess Rate (%)		24.9	7.0	7.8 34.8 Baseline (Qwen2.5-VL-3B-Instruct) Cross-Task (SFT + RL) 10-Task (SFT + RL) 20.2 25.0 11.5 13.2 12.0 7.9 4.6	
Overall Results on H 0	Easy OS task ac	ross Di	Medium fficulty Lev		Hard		Ov	erall Re	Easy sults on <i>HP</i>	Medium Hard Extreme St task across Difficulty Levels	

Figure 4. Comparison of In-task (train and test on the same task family) and Cross-task (train on one task family and test on the other).

HPS, difficulty depends on whether the scene contains textual cues and whether the visual or textual cues align with the actual path direction. These two factors jointly define four difficulty levels (see Fig. 3 Bottom Right; visualizations in Fig. IV-Fig. VII).

5. Experiment

5.1. Experiment Setup

Implementation Details. (1) *Training Setup*: We finetune the model on a mixed object and path search dataset. The SFT training environment is implemented with LLaMA-Factory [69], and the RL training is built on an open-source framework VAGEN [57]. The full training details can be found in Appendix VI for more details. We perform fullparameter SFT on Qwen2.5-VL-3B-Instruct for 3 epochs; the resulting model is HVS-3B (w/ SFT only). For the RL stage, we train with RL for 70 steps. We denote the obtained model as HVS-3B. The prompts used in our experiments are provided in Appendix Fig. II. (2) Benchmark Setup: We evaluate open-source and proprietary models that support multi-image input. We use the same evaluation environment as RL training. See Appendix for the detailed training-test split for the proposed two tasks. Evaluation Metric. A trial is evaluated as success if the submitted final viewing direction $(\dot{\phi}, \hat{\gamma})$ falls inside a bbox-centered tolerance region $[\phi^* - \tau_{\phi}, \phi^* + \tau_{\phi}] \times [\gamma^* - \tau_{\gamma}, \gamma^* + \tau_{\gamma}]$ around the objective direction (ϕ^*, γ^*) (the spherical direction of annotated bbox center). The parameters of tolerance are defined

as: $\tau_{\phi} = \max(\frac{w_{\phi}}{2}, \tau_{\phi})$ and $\tau_{\gamma} = \max(\frac{w_{\gamma}}{2}, \tau_{\gamma})$, where w_{ϕ} and w_{γ} are the angular width and height of the bounding box. Following Sec. 3.1, $(\hat{\phi}, \hat{\gamma})$ are evaluated for HOS task, whereas for HOS we assess only $(\hat{\phi})$. The tolerances are $\tau_{\phi} = 30^{\circ}, \tau_{\gamma} = 20^{\circ}$ for HOS (to mimic the human foveation) and $\tau_{\phi} = 10^{\circ}$ for HPS (to reflect the requirement for precise motion direction). We report success rate (%) by task and difficulty.

5.2. Probing Embodied Visual Search in MLLMs

Main Results. Table 1 shows a large performance gap between proprietary and open-weight models, with Gemini2.5-Pro standing out as the strongest overall performer in *HOS* (31.96) and *HPS* (33.00). The Gemma-3 series achieves the best results among open-weight models. Interestingly, a larger model size does not guarantee better performance. For both the Gemma-3 and Qwen2.5-VL series, the smaller 4B/3B models surpass their larger 12B/7B counterparts in *HOS*, while performing on par in *HPS*.

Error Analysis. In *HOS*, errors arise from (1) *limited visual grounding capabilities* (*e.g.*, the agent fails to reliably identify targets in cluttered environments), and (2) *perception-action gap* (*e.g.*, agent detects a target but cannot perform fine-grained foveation). In *HPS*, we identify three types of errors: (1) *vision-action mismatch*: The model perceives visual cues (*e.g.*, signs) but fails to translate them into physical actions; (2) *lack of physical commonsense*: Actions violate 3D constraints (*e.g.*, attempting



Figure 5. Left: Failure cases in *HPS*. (a) Vision-action mismatch. (b) Attempting to traverse an impassable surface instead of using an adjacent staircase. (c) Missing socio-spatial conventions (*e.g.*, airport entrance cues), resulting in a fruitless search. **Right:** *H*Bench* results breakdown of Gemma3-4B-it.

to pass through walls); (3) lack of socio-spatial commonsense: The model misses implicit rules and norms of built environments (e.g., the function of stairs, police tape, and crosswalks), as shown in Fig. 5 Left. The breakdown of results is shown in Fig. 5 Right, and additional examples are provided in Appendix Sec. VII. These findings suggest:

MLLMs can form linguistically grounded spatial models for passive world description, but not physically grounded ones for embodied world interaction.

5.3. On the Role and Limits of Post-Training

Effectiveness of SFT and RL. Our post-training framework demonstrates significant improvements over the base model. As shown in Tab. 1, SFT contributes the majority of performance gains: on HOS, SFT alone improves the overall score from 14.83 to 40.83 (\uparrow 26.00), while on **HPS**, it elevates performance from 6.44 to 23.00 (\(\frac{1}{6}.56 \)). Subsequent RL provides additional but more modest gains: \\$\footnote{6.55}\$ on object search and \$\frac{1}{2}\$. 94 on path search. This indicates that SFT establishes the fundamental task capability, while RL serves as a refinement step for further optimization. Specifically, we find that post-training improves several key abilities: (1) precise control over rotation angles, (2) the use of large-angle turns to explore new areas, and (3) the capacity to act on directional signs (see Appendix VIII for case studies). In addition, applying RL directly without prior SFT degrades the instruction following capability of the models.

Task-Dependent Efficacy. The benefits of post-training vary by task complexity. For the simpler object search, our model (47.38) outperforms the state-of-the-art proprietary model Gemini2.5-Pro (31.96). Yet for the more complex

path search, its absolute score (24.94) falls short of the art (33.00). This gap suggests that *post-training has limitations* in enhancing higher-order spatial reasoning capabilities.

Negative Impact of RL on Complex Tasks. In *HPS*, RL reduces performance on *medium* difficulty from 23.03 to 20.18 and on *extreme* difficulty from 14.81 to 12.04. These scenarios are characterized by a misalignment between visual cues and the optimal path, a pattern our taxonomy identifies as rather challenging. We hypothesise that this degradation may stem from reward hacking, where the model learns to exploit the reward signal rather than genuinely improving its reasoning capability. *This highlights the challenge of designing reward functions that consistently align with true task objectives across all difficulty levels*.

Key Takeaway. The disparate impact of our post-training method on object versus path search is telling. While SFT+RL yields substantial gains in object search across all difficulty levels, its improvements on the more demanding path search are more modest, with RL even degrading performance on some hard cases. This pattern suggests that:

Post-training can improve visual grounding and exploration for object search, but struggles to impart physical, spatial, and social commonsense for path search, as these are often implicit, situational, and procedural.

5.4. Dissecting Object and Path Search

In-Task Superiority with an Exception. As shown in Fig. 4, in-task training delivers peak performance, with one exception: a model trained on object search achieves 37.8% on the *easy HPS* split, surpassing both the baseline (7.0%) and the dedicated in-task *HPS* model (33.8%). We hypoth-

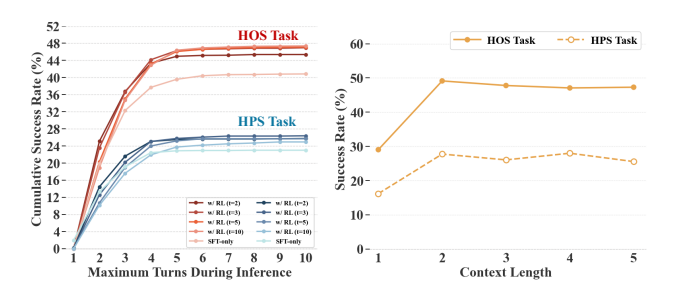


Figure 6. **Left:** Cumulative success rate by step before and after RL (t indicates maximum turn limit in RL training). **Right:** Impact of test-time context length on success rate.

	Humanoid Path Search								
Method	Overall	Easy	Medium	Hard	Extreme				
GRPO on HPS									
sft (baseline)	23.44	26.00	24.56	24.77	12.50				
form+corr	22.38	33.80	17.32	21.73	7.87				
form+corr+dist	21.37	34.40	15.13	20.09	6.94				
form+dist	21.31	29.80	17.54	20.56	11.11				

Table 2. Results of GRPO with different reward shaping on HPS.

esize that these easy tasks reduce to simple object searches where clear visual cues define the path, allowing the powerful object-finding skills from **HOS** to transfer effectively. Cross-Task Generalization. We observe a clear bidirectional synergy: training on object search boosts path search performance from 6.4% to 20.7%, while training on path search elevates object search from 14.8% to 29.5%. This is because skills acquired from learning path search, like active exploration and path reasoning, confer a direct performance advantage in object search, while the visual grounding honed in object search reciprocally benefits path search. Mixed-Data Training. Training on a mixed object and path search dataset yields the best overall performance. Yet this comes with a key challenge: performance gains are unevenly distributed, as improvements on certain splits can reduce performance on others. Balancing this trade-off is essential for developing generalist humanoid agents.

5.5. Ablation Study

Reward Shaping. We ablate three types of rewards for path search: (1) format + correctness, (2) format + correctness + distance-to-goal, and (3) format + distance-to-goal (see Appendix V for reward functions). All variants improve performance only on the *easy* split, often degrading harder levels (Tab. 2). This underlines the difficulty of path search and the need for more advanced learning algorithms.

Training Rollout and Context Length. As Fig. 6 shows, models trained with short GRPO rollouts can achieve satisfactory performance through test-time scaling, and match the performance of models trained with longer rollouts (10 turns) while converging faster. This ensure training efficiency without sacrificing final performance. Meanwhile, a short context length of 2 rounds is enough on *HVS*.

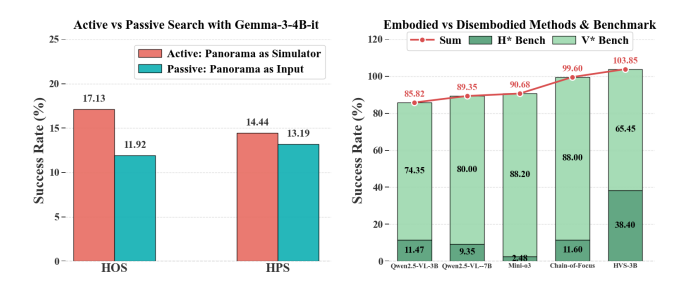


Figure 7. **Left:** Comparison of active and passive visual search. **Right:** Comparison of different visual search paradigms.

Active vs. Passive. We compare active visual search, where an agent with a perspective view rotates to gather information, against the passive analysis of a complete panorama. The active paradigm is superior for two key reasons: (1) it mirrors efficient, human-like search strategies, and (2) it avoids panoramic distortions that conflict with MLLM training priors. Our empirical results validate this superiority; using Gemma-3-4B-it, we find the passive approach can degrade the performance (Fig. 7 Left). In addition, this emphasis on active spatial intelligence aligns our work with a growing body of research on active vision [26, 62].

Embodied vs. Disembodied Bench. As shown in Fig. 7 Right, 2D methods like Mini-o3 [29] and Chainof-Focus [67] achieve near-saturation performance on the disembodied V^* Bench (88.2% and 88.0%, respectively), indicating that visual search within a static 2D image is no longer challenging for MLLMs. However, their performance plummets on our embodied H^*Bench , with success rates dropping to a mere 2.5% and 11.6%. This stark contrast demonstrates that capabilities learned from passive Internet data do not transfer to embodied active interaction in 3D. Actually, our HVS-3B model achieves a success rate of only 38.4%, highlighting that HVS remains a wide-open research problem. Notably, our model maintains a satisfactory 65.5% success rate on V^* **Bench**. This suggests that:

Our model learns 3D embodied search without compromising its 2D visual search ability too much, indicating a promising path toward a unified model capable of operating in both physical and digital realms.

6. Discussion and Future Work

We study MLLM-powered humanoid visual search in the wild by introducing the H^*Bench and leveraging post-training to enhance the performance. Our analysis reveals that while post-training effectively improves low-level perceptual-motor abilities—such as visual grounding and exploration—it exposes fundamental bottlenecks in higher-level reasoning, which requires physical, spatial, and social commonsense. Furthermore, while RL boosts performance on simpler tasks, it can paradoxically degrade performance

in complex scenarios. Future work should focus on designing more robust reward functions as well as more efficient vision tokenizers, developing pre-training methods that instill action-oriented spatial world knowledge, and balancing performance across task difficulties. Meanwhile, scaling up the collection of embodied search data is essential for fully unlocking visual-spatial reasoning in the wild.

Acknowledgment. The work was supported in part through NSF grants 2514030, 2238968, 2345139, 2443404, and the NYU IT High Performance Computing resources, services, and staff expertise. S.X. acknowledges support from the MSIT ITP grant (RS-2024-00457882). The authors thank Justin Kerr and Ken Goldberg for insightful discussion.

References

- [1] Jean-Baptiste Alayrac, Jeff Donahue, Pauline Luc, Antoine Miech, Iain Barr, Yana Hasson, Karel Lenc, Arthur Mensch, Katherine Millican, Malcolm Reynolds, et al. Flamingo: a visual language model for few-shot learning. Advances in neural information processing systems, 35:23716–23736, 2022. 3
- [2] Peter Anderson, Qi Wu, Damien Teney, Jake Bruce, Mark Johnson, Niko Sünderhauf, Ian Reid, Stephen Gould, and Anton Van Den Hengel. Vision-and-language navigation: Interpreting visually-grounded navigation instructions in real environments. In *Proceedings of the IEEE conference on computer vision and pattern recognition*, pages 3674–3683, 2018. 3
- [3] Alisson Azzolini, Junjie Bai, Hannah Brandon, Jiaxin Cao, Prithvijit Chattopadhyay, Huayu Chen, Jinju Chu, Yin Cui, Jenna Diamond, Yifan Ding, et al. Cosmos-reason1: From physical common sense to embodied reasoning. *arXiv* preprint arXiv:2503.15558, 2025. 3
- [4] Graham R Barnes. Vestibulo-ocular function during coordinated head and eye movements to acquire visual targets. *The Journal of Physiology*, 287(1):127–147, 1979. 3
- [5] Albert E Bartz. Eye and head movements in peripheral vision: nature of compensatory eye movements. *Science*, 152 (3729):1644–1645, 1966. 2
- [6] Jake Bruce, Michael D Dennis, Ashley Edwards, Jack Parker-Holder, Yuge Shi, Edward Hughes, Matthew Lai, Aditi Mavalankar, Richie Steigerwald, Chris Apps, et al. Genie: Generative interactive environments. In Forty-first International Conference on Machine Learning, 2024. 2
- [7] Matthew Chang, Théophile Gervet, Mukul Khanna, Sriram Yenamandra, Dhruv Shah, So Yeon Min, Kavit Shah, Chris Paxton, Saurabh Gupta, Dhruv Batra, et al. Goat: Go to any thing. In *Robotics: Science and Systems*, 2024. 3
- [8] Devendra Singh Chaplot, Dhiraj Gandhi, Saurabh Gupta, Abhinav Gupta, and Ruslan Salakhutdinov. Learning to explore using active neural slam. In 8th International Conference on Learning Representations, 2020.
- [9] Devendra Singh Chaplot, Dhiraj Prakashchand Gandhi, Abhinav Gupta, and Russ R Salakhutdinov. Object goal navigation using goal-oriented semantic exploration. Advances

- in Neural Information Processing Systems, 33:4247–4258, 2020.
- [10] Devendra Singh Chaplot, Ruslan Salakhutdinov, Abhinav Gupta, and Saurabh Gupta. Neural topological slam for visual navigation. In *Proceedings of the IEEE/CVF conference* on computer vision and pattern recognition, pages 12875– 12884, 2020. 3
- [11] Hao Chen, Yuqi Hou, Chenyuan Qu, Irene Testini, Xiaohan Hong, and Jianbo Jiao. 360+x: A panoptic multimodal scene understanding dataset. In *Proceedings of the IEEE/CVF Conference on Computer Vision and Pattern Recognition*, 2024. 5
- [12] William Chen, Suneel Belkhale, Suvir Mirchandani, Oier Mees, Danny Driess, Karl Pertsch, and Sergey Levine. Training strategies for efficient embodied reasoning. arXiv preprint arXiv:2505.08243, 2025. 3
- [13] Zhe Chen, Bin Fu, Junjun He, Yu Qiao, Dahua Lin, Limin Wang, Xizhou Zhu, Weijie Su, Jifeng Dai, Yinan He, and et al. Internvl3.5: Advancing open-source multimodal models in versatility, reasoning, and efficiency, 2025. 6
- [14] Tianzhe Chu, Yuexiang Zhai, Jihan Yang, Shengbang Tong, Saining Xie, Dale Schuurmans, Quoc V Le, Sergey Levine, and Yi Ma. Sft memorizes, rl generalizes: A comparative study of foundation model post-training. In Forty-second International Conference on Machine Learning, 2025. 4
- [15] Matt Deitke, Eli VanderBilt, Alvaro Herrasti, Luca Weihs, Kiana Ehsani, Jordi Salvador, Winson Han, Eric Kolve, Aniruddha Kembhavi, and Roozbeh Mottaghi. Procthor: Large-scale embodied ai using procedural generation. In Advances in Neural Information Processing Systems, pages 5982–5994, 2022. 2
- [16] Alexey Dosovitskiy, German Ros, Felipe Codevilla, Antonio Lopez, and Vladlen Koltun. Carla: An open urban driving simulator. In *Conference on robot learning*, pages 1–16. PMLR, 2017.
- [17] Lang Feng, Zhenghai Xue, Tingcong Liu, and Bo An. Group-in-group policy optimization for llm agent training. arXiv preprint arXiv:2505.10978, 2025. 3
- [18] Wei Fu, Jiaxuan Gao, Xujie Shen, Chen Zhu, Zhiyu Mei, Chuyi He, Shusheng Xu, Guo Wei, Jun Mei, Jiashu Wang, et al. Areal: A large-scale asynchronous reinforcement learning system for language reasoning. *arXiv preprint arXiv:2505.24298*, 2025. 3
- [19] Gemma Team, Aishwarya Kamath, Johan Ferret, Shreya Pathak, Nino Vieillard, Ramona Merhej, Sarah Perrin, Tatiana Matejovicova, Alexandre Ramé, Morgane Rivière, Louis Rouillard, and et al. Gemma 3 technical report, 2025.
- [20] Daya Guo, Dejian Yang, Haowei Zhang, Junxiao Song, Ruoyu Zhang, Runxin Xu, Qihao Zhu, Shirong Ma, Peiyi Wang, Xiao Bi, et al. Deepseek-r1: Incentivizing reasoning capability in Ilms via reinforcement learning. arXiv preprint arXiv:2501.12948, 2025. 3
- [21] Junxian He, Heng Ji, Yan Ma, Yu Cheng, Zhengyuan Yang, Linjie Li, Hangyu Guo, Jiaqi Liu, Xiaoye Qu, Zhenhua Liu, Peng Xia, Zhaochen Su, Yanshu Li, Yi R., Fung, and Kaide Zeng. Thinking with images for multimodal reasoning: Foundations, methods, and future frontiers, 2025. 4

- [22] Wenxuan Huang, Bohan Jia, Zijie Zhai, Shaosheng Cao, Zheyu Ye, Fei Zhao, Zhe Xu, Yao Hu, and Shaohui Lin. Vision-r1: Incentivizing reasoning capability in multimodal large language models. arXiv preprint arXiv:2503.06749, 2025. 3
- [23] Jyh-Jing Hwang, Runsheng Xu, Hubert Lin, Wei-Chih Hung, Jingwei Ji, Kristy Choi, Di Huang, Tong He, Paul Covington, Benjamin Sapp, et al. Emma: End-to-end multimodal model for autonomous driving. arXiv preprint arXiv:2410.23262, 2024. 3
- [24] Bowen Jin, Hansi Zeng, Zhenrui Yue, Jinsung Yoon, Sercan Arik, Dong Wang, Hamed Zamani, and Jiawei Han. Searchr1: Training llms to reason and leverage search engines with reinforcement learning. arXiv preprint arXiv:2503.09516, 2025. 3
- [25] Daniel Kahneman. Thinking, fast and slow. macmillan, 2011. 2
- [26] Justin Kerr, Kush Hari, Ethan Weber, Chung Min Kim, Brent Yi, tyler bonnen, Ken Goldberg, and Angjoo Kanazawa. Eye, robot: Learning to look to act with a bc-rl perception-action loop. In *Proceedings of The 9th Conference on Robot Learn*ing, pages 3647–3664. PMLR, 2025. 8
- [27] Team Kimi, Angang Du, Bofei Gao, Bowei Xing, Changjiu Jiang, Cheng Chen, Cheng Li, Chenjun Xiao, Chenzhuang Du, Chonghua Liao, et al. Kimi k1. 5: Scaling reinforcement learning with llms. arXiv preprint arXiv:2501.12599, 2025.
- [28] Team Kimi, Angang Du, Bohong Yin, Bowei Xing, Bowen Qu, Bowen Wang, Cheng Chen, Chenlin Zhang, Chenzhuang Du, Chu Wei, et al. Kimi-vl technical report. arXiv preprint arXiv:2504.07491, 2025. 3
- [29] Xin Lai, Junyi Li, Wei Li, Tao Liu, Tianjian Li, and Hengshuang Zhao. Mini-o3: Scaling up reasoning patterns and interaction turns for visual search. *arXiv preprint* arXiv:2509.07969, 2025. 8
- [30] Jeremy Lanman, Emilio Bizzi, and John Allum. The coordination of eye and head movement during smooth pursuit. *Brain research*, 153(1):39–53, 1978. 3
- [31] Chengshu Li, Ruohan Zhang, Josiah Wong, Cem Gokmen, Sanjana Srivastava, Roberto Martín-Martín, Chen Wang, Gabrael Levine, Michael Lingelbach, Jiankai Sun, et al. Behavior-1k: A benchmark for embodied ai with 1,000 everyday activities and realistic simulation. In *Conference on Robot Learning*, pages 80–93. PMLR, 2023. 2
- [32] Geng Li, Jinglin Xu, Yunzhen Zhao, and Yuxin Peng. Dyfo: A training-free dynamic focus visual search for enhancing lmms in fine-grained visual understanding. In *Proceedings* of the Computer Vision and Pattern Recognition Conference, pages 9098–9108, 2025. 2
- [33] Junnan Li, Dongxu Li, Caiming Xiong, and Steven Hoi. Blip: Bootstrapping language-image pre-training for unified vision-language understanding and generation. In *International Conference on Machine Learning*, pages 12888–12900. PMLR, 2022. 3
- [34] Junnan Li, Dongxu Li, Silvio Savarese, and Steven Hoi. Blip-2: Bootstrapping language-image pre-training with frozen image encoders and large language models. In *In-*

- ternational Conference on Machine Learning, pages 19730–19742. PMLR, 2023. 3
- [35] Haotian Liu, Chunyuan Li, Qingyang Wu, and Yong Jae Lee. Visual instruction tuning. In *NeurIPS*, 2023. 3
- [36] Zuyan Liu, Yuhao Dong, Yongming Rao, Jie Zhou, and Jiwen Lu. Chain-of-spot: Interactive reasoning improves large vision-language models. arXiv preprint arXiv:2403.12966, 2024. 3
- [37] Arjun Majumdar, Gunjan Aggarwal, Bhavika Devnani, Judy Hoffman, and Dhruv Batra. Zson: Zero-shot object-goal navigation using multimodal goal embeddings. Advances in Neural Information Processing Systems, 35:32340–32352, 2022. 3
- [38] Yunze Man, De-An Huang, Guilin Liu, Shiwei Sheng, Shilong Liu, Liang-Yan Gui, Jan Kautz, Yu-Xiong Wang, and Zhiding Yu. Argus: Vision-centric reasoning with grounded chain-of-thought. In Proceedings of the Computer Vision and Pattern Recognition Conference, pages 14268–14280, 2025.
- [39] David Marr. Vision: A computational investigation into the human representation and processing of visual information. MIT press, 2010. 2
- [40] Aude Oliva, Antonio Torralba, Monica S Castelhano, and John M Henderson. Top-down control of visual attention in object detection. In *Proceedings 2003 international conference on image processing (Cat. No. 03CH37429)*, pages I–253. IEEE, 2003. 2
- [41] OpenAI. Hello gpt-4o. Blog, 2024. Accessed: November 22, 2024. 3, 4, 5, 6
- [42] OpenManus. Openmanus-rl: Open platform for generalist llm reasoning agents with rl optimization, 2025. 3
- [43] Long Ouyang, Jeffrey Wu, Xu Jiang, Diogo Almeida, Carroll Wainwright, Pamela Mishkin, Chong Zhang, Sandhini Agarwal, Katarina Slama, Alex Ray, et al. Training language models to follow instructions with human feedback. pages 27730–27744, 2022. 3
- [44] Ji Qi, Ming Ding, Weihan Wang, Yushi Bai, Qingsong Lv, Wenyi Hong, Bin Xu, Lei Hou, Juanzi Li, Yuxiao Dong, et al. Cogcom: A visual language model with chain-ofmanipulations reasoning. In *ICLR*, 2025. 3
- [45] Zhangyang Qi, Zhixiong Zhang, Yizhou Yu, Jiaqi Wang, and Hengshuang Zhao. Vln-r1: Vision-language navigation via reinforcement fine-tuning. *arXiv* preprint arXiv:2506.17221, 2025. 3
- [46] Dorsa Sadigh, Arvind Neelakantan, Pranav Shyam, Noam Shazeer, Archit Sharma, Naman Goyal, Yossi Matias, Lawrence Chan, Zhe Chen, and et al. Gemini 2.5: Pushing the frontier with advanced reasoning, multimodality, long context, and next generation agentic capabilities, 2025. 3,
- [47] Manolis Savva, Abhishek Kadian, Oleksandr Maksymets, Yili Zhao, Erik Wijmans, Bhavana Jain, Julian Straub, Jia Liu, Vladlen Koltun, Jitendra Malik, et al. Habitat: A platform for embodied ai research. In Proceedings of the IEEE/CVF international conference on computer vision, pages 9339–9347, 2019. 2
- [48] Zhihong Shao, Peiyi Wang, Qihao Zhu, R. Xu, Jun-Mei Song, Mingchuan Zhang, Y. K. Li, Yu Wu, and Daya Guo.

- Deepseekmath: Pushing the limits of mathematical reasoning in open language models. *ArXiv*, abs/2402.03300, 2024.
- [49] Haozhan Shen, Kangjia Zhao, Tiancheng Zhao, Ruochen Xu, Zilun Zhang, Mingwei Zhu, and Jianwei Yin. Zoomeye: Enhancing multimodal llms with human-like zooming capabilities through tree-based image exploration. *arXiv preprint arXiv:2411.16044*, 2024. 3
- [50] Grayden JF Solman, Tom Foulsham, and Alan Kingstone. Eye and head movements are complementary in visual selection. *Royal Society Open Science*, 4(1):160569, 2017.
- [51] Alex Su, Haozhe Wang, Weiming Ren, Fangzhen Lin, and Wenhu Chen. Pixel reasoner: Incentivizing pixel-space reasoning with curiosity-driven reinforcement learning. *arXiv* preprint arXiv:2505.15966, 2025. 2
- [52] Gemini Robotics Team, Saminda Abeyruwan, Joshua Ainslie, Jean-Baptiste Alayrac, Montserrat Gonzalez Arenas, Travis Armstrong, Ashwin Balakrishna, Robert Baruch, Maria Bauza, Michiel Blokzijl, et al. Gemini robotics: Bringing ai into the physical world. *arXiv preprint arXiv:2503.20020*, 2025. 3
- [53] Kimi Team. Kimi-vl technical report, 2025. 6
- [54] Xiaoyu Tian, Junru Gu, Bailin Li, Yicheng Liu, Yang Wang, Zhiyong Zhao, Kun Zhan, Peng Jia, XianPeng Lang, and Hang Zhao. Drivevlm: The convergence of autonomous driving and large vision-language models. In *Conference on Robot Learning*, pages 4698–4726. PMLR, 2025. 3
- [55] Peter Tong, Ellis Brown, Penghao Wu, Sanghyun Woo, Adithya Jairam Vedagiri IYER, Sai Charitha Akula, Shusheng Yang, Jihan Yang, Manoj Middepogu, Ziteng Wang, et al. Cambrian-1: A fully open, vision-centric exploration of multimodal llms. Advances in Neural Information Processing Systems, 37:87310–87356, 2024. 3
- [56] Antonio Torralba, Aude Oliva, Monica S Castelhano, and John M Henderson. Contextual guidance of eye movements and attention in real-world scenes: the role of global features in object search. *Psychological review*, 113(4):766, 2006. 2
- [57] Kangrui Wang, Pingyue Zhang, Zihan Wang, Yaning Gao, Linjie Li, Qineng Wang, Hanyang Chen, Chi Wan, Yiping Lu, Zhengyuan Yang, Lijuan Wang, Ranjay Krishna, Jiajun Wu, Li Fei-Fei, Yejin Choi, and Manling Li. Reinforcing visual state reasoning for multi-turn vlm agents, 2025. 6
- [58] Penghao Wu and Saining Xie. V*: Guided visual search as a core mechanism in multimodal llms. In *Proceedings of* the IEEE/CVF Conference on Computer Vision and Pattern Recognition, pages 13084–13094, 2024. 2
- [59] Wayne Wu, Honglin He, Jack He, Yiran Wang, Chenda Duan, Zhizheng Liu, Quanyi Li, and Bolei Zhou. Metaurban: An embodied ai simulation platform for urban micromobility. *International Conference on Learning Representation*, 2025. 2
- [60] Fei Xia, Amir R Zamir, Zhiyang He, Alexander Sax, Jitendra Malik, and Silvio Savarese. Gibson env: Real-world perception for embodied agents. In *Proceedings of the IEEE con*ference on computer vision and pattern recognition, pages 9068–9079, 2018. 2

- [61] Yiheng Xu, Peng Wang, Hang Zhang, Pengfei Wang, Shuai Bai, Shijie Wang, Junyang Lin, Tianbao Xie, Yuanzhi Zhu, Zhibo Yang, and et al. Qwen2.5-vl technical report, 2025. 6
- [62] Justin Yu, Yide Shentu, Di Wu, Pieter Abbeel, Ken Goldberg, and Philipp Wu. Egomi: Learning active vision and whole-body manipulation from egocentric human demonstrations. *arXiv* preprint arXiv:2511.00153, 2025. 8
- [63] Tianyu Yu, Yuan Yao, Haoye Zhang, Taiwen He, Yifeng Han, Ganqu Cui, Jinyi Hu, Zhiyuan Liu, Hai-Tao Zheng, Maosong Sun, et al. Rlhf-v: Towards trustworthy mllms via behavior alignment from fine-grained correctional human feedback. In Proceedings of the IEEE/CVF Conference on Computer Vision and Pattern Recognition, pages 13807– 13816, 2024. 3
- [64] Michał Zawalski, William Chen, Karl Pertsch, Oier Mees, Chelsea Finn, and Sergey Levine. Robotic control via embodied chain-of-thought reasoning. In *Conference on Robot Learning*, pages 3157–3181. PMLR, 2025. 3
- [65] Gregory Zelinsky, Wei Zhang, Bing Yu, Xin Chen, and Dimitris Samaras. The role of top-down and bottom-up processes in guiding eye movements during visual search. In *Advances in neural information processing systems*, 2005. 2
- [66] Jiarui Zhang, Mahyar Khayatkhoei, Prateek Chhikara, and Filip Ilievski. Mllms know where to look: Training-free perception of small visual details with multimodal llms. In *The Thirteenth International Conference on Learning Represen*tations, 2025. 2
- [67] Xintong Zhang, Zhi Gao, Bofei Zhang, Pengxiang Li, Xiaowen Zhang, Yang Liu, Tao Yuan, Yuwei Wu, Yunde Jia, Song-Chun Zhu, et al. Chain-of-focus: Adaptive visual search and zooming for multimodal reasoning via rl. arXiv preprint arXiv:2505.15436, 2025. 2, 3, 8
- [68] Qingqing Zhao, Yao Lu, Moo Jin Kim, Zipeng Fu, Zhuoyang Zhang, Yecheng Wu, Zhaoshuo Li, Qianli Ma, Song Han, Chelsea Finn, et al. Cot-vla: Visual chain-of-thought reasoning for vision-language-action models. In *Proceedings* of the Computer Vision and Pattern Recognition Conference, pages 1702–1713, 2025. 3
- [69] Yaowei Zheng, Richong Zhang, Junhao Zhang, Yanhan Ye, Zheyan Luo, Zhangchi Feng, and Yongqiang Ma. Llamafactory: Unified efficient fine-tuning of 100+ language models. In Proceedings of the 62nd Annual Meeting of the Association for Computational Linguistics (Volume 3: System Demonstrations), Bangkok, Thailand, 2024. Association for Computational Linguistics. 6
- [70] Ziwei Zheng, Michael Yang, Jack Hong, Chenxiao Zhao, Guohai Xu, Le Yang, Chao Shen, and Xing Yu. Deepeyes: Incentivizing" thinking with images" via reinforcement learning. arXiv preprint arXiv:2505.14362, 2025. 3
- [71] Gengze Zhou, Yicong Hong, Zun Wang, Xin Eric Wang, and Qi Wu. Navgpt-2: Unleashing navigational reasoning capability for large vision-language models. In *European Con*ference on Computer Vision, pages 260–278, 2024. 3
- [72] Yuke Zhu, Roozbeh Mottaghi, Eric Kolve, Joseph J Lim, Abhinav Gupta, Li Fei-Fei, and Ali Farhadi. Target-driven visual navigation in indoor scenes using deep reinforcement learning. In 2017 IEEE international conference on robotics and automation (ICRA), pages 3357–3364. IEEE, 2017. 3

Appendix

I. Geographical Distribution of H*Bench

As shown in Fig. I, our dataset exhibits broad geographical coverage, including thirteen cities across twelve countries and four continents. This diversity is reflected in the wide range of architectural styles, languages and scripts on signage, and environmental conditions.

II. HVS Task Difficulty Visualization

II.1. HOS Difficulty Visualization

Figure III illustrates the three difficulty levels of our *HOS* task with concrete examples. For each keyframe, we overlay the target object's area on the initial view and provide its visibility ratio *d*. From left to right, we show one example per level: **Easy** (mostly visible), **Medium** (partially visible), and **Hard** (invisible), demonstrating the model's initial observation.

II.2. HPS Difficulty Visualization

We define the four difficulty levels of the *HPS* task based on two criteria: whether the relevant cue aligns with the navigable path and whether textual information is provided. Examples are shown in Fig. IV-Fig. VII.

III. Training and Inference Prompts

The natural-language prompts used for training and inference of the *HOS* and *HPS* tasks are shown in Fig. II.

IV. Objective Functions

SFT stage. The SFT objective function is the expected negative log-likelihood (cross-entropy loss) over the dataset \mathcal{D}^{SFT} which consists of task input x and labeled trajectory \mathcal{H}_T :

$$\min_{\theta} \mathbb{E}_{(x,\mathcal{H}_T) \sim \mathcal{D}^{SFT}} \left[-\sum_{i=0}^{T-1} \log \pi_{\theta}(y_i, a_i \mid o_i, x, \mathcal{H}_i) \right].$$

RL stage. For each task, we sample G times and get outputs $\{\omega_1,\omega_2,\ldots,\omega_G\}$ where ω_i includes all the output tokens in the output sequence $\{y_0,a_0,y_1,a_1,\ldots,y_{T-1},a_{T-1}\}$, then calculate the GRPO advantage to update the parameters. The GRPO objective function is:

$$\begin{split} &\mathcal{J}_{\text{GRPO}}(\theta) = \mathbb{E}[(s_o, x, y) \sim \mathcal{D}^{RL}, \{\omega_i\}_{i=1}^G \sim \pi_{\theta_{\text{old}}}(\Omega|s_o, x)] \\ &\frac{1}{G} \sum_{i=1}^G \frac{1}{|\omega_i|} \sum_{t=1}^{|\omega_i|} \\ &\left\{ \min \left[\frac{\pi_{\theta}(\omega_{i,t}|s_o, x, \omega_{i, < t})}{\pi_{\theta_{\text{old}}}(\omega_{i,t}|s_o, x, \omega_{i, < t})} \hat{A}_{i,t}, \text{clip}(\frac{\pi_{\theta}(\omega_{i,t}|s_o, x, \omega_{i, < t})}{\pi_{\theta_{\text{old}}}(\omega_{i,t}|s_o, x, \omega_{i, < t})} \right. \\ &\left. , 1 - \epsilon, 1 + \epsilon) \hat{A}_{i,t} \right] - \beta \, \mathbb{KL}(\pi_{\theta} \| \pi_{\text{ref}}) \right\}, \end{split}$$

where $\hat{A}_{i,t}$ denotes the group relative advantage at $\omega_{i,t}$:

$$\hat{A}_{i,t} = \frac{r_i - \text{mean}(r)}{\text{std}(r)}.$$

V. Reward Shaping

We use rule-based reward function to calculate the reward of the trajectory, which includes correctness reward, format reward.

$$r = r_{corr} + r_{form},$$

where:

$$r_{\rm corr} = \begin{cases} 0.5, & \text{if the submitted answer satisfies the} \\ & \text{completion condition,} \\ 0, & \text{otherwise,} \end{cases}$$

$$r_{\rm form} = \begin{cases} 0.5, & \text{if the response is in $<$think}> \\ & <{\rm answer}>{\rm canswer}>{\rm format}, \\ 0, & \text{otherwise}. \end{cases}$$

Specially, we add a distance-to-goal reward for *HPS*. It is calculated by the distance of the final direction to the target bounding box.

$$r_{dist} = \frac{\pi - d(\phi_T, \phi^*) + \pi - d(\gamma_T, \gamma^*)}{2\pi}.$$

Distance to bounding box is calculated by:

$$d(\alpha, \alpha^*) = |\alpha - (\alpha^* - \tau_\alpha)| + |\alpha - (\alpha^* + \tau_\alpha)|$$

which remains a constant minimum value when the direction is in the bounding box.

VI. Experimental Setup

Training Details. For the SFT stage, we use a learning rate of 1e-5. For the RL stage, we apply the GRPO algorithm with a batch size of 32, an actor learning rate of 1×10^{-7} , and a KL penalty coefficient $\beta=0.01$. Rollouts are conducted under the H^*Bench prompts with a temperature of 0.7, a maximum of 8 trajectories, and a dynamic turn limit (5 or 10) based on computational resources. Both stages use an input resolution of 1280×720 and are run on 8 NVIDIA H100 GPUs.

Benchmark Setting. The maximum number of inference turns is set to 10, as the step-cumulative success rate converges before this limit. At each step, the model processes up to five perspective images and uses the latest five dialogue turns as context. The image resolution is 1920×1080 , and the sampling temperature is 0. Due to computational constraints, each episode is capped at 10 steps, with unfinished episodes counted as failures.

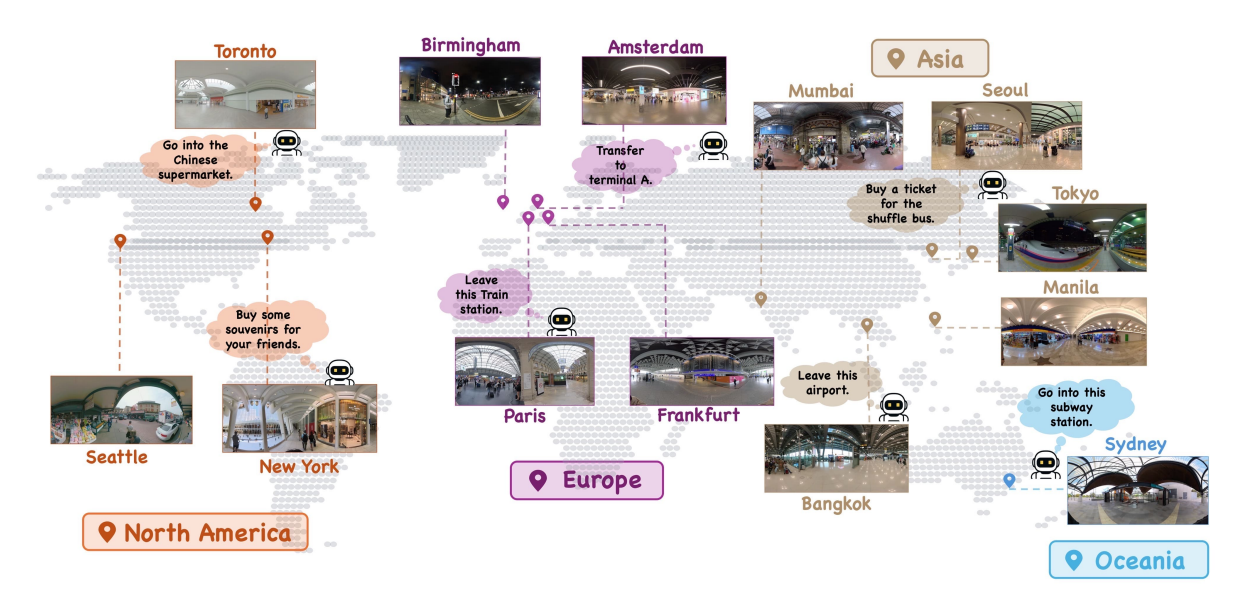


Figure I. H*Bench aggregates panoramic videos from diverse global locations, featuring visually cluttered environments.

Train-Test Split. We annotated $\sim 3,000$ task instances. These were divided into three mutually exclusive splits per task: a benchmark split, an SFT split, and an RL training split. Specifically, we reserved 1,000 instances (600 *HOS* and 400 *HPS*) as the H^*Bench , resulting in 4,000 evaluation episodes. From the remaining data, we constructed the SFT dataset by randomly sampling 250 instances from both the *HOS* and *HPS* pools. All leftover instances were allocated exclusively for RL training.

VII. Additional Qualitative Error Analysis

In Section 5.2, we identified two common-sense reasoning errors in the *HPS* task: (1) *lack of physical commonsense* and (2) *lack of socio-spatial commonsense*. This section provides a detailed explanation of these error types, supported by additional qualitative examples.

Lack of Physical Commonsense. This error type denotes a failure in applying intuitive knowledge about 3D geometry and basic physics. Potential failures caused by the lack of physical commonsense include:

- **Ignoring Permanent Obstacles:** Attempting to move through non-traversable objects such as solid walls, glass barriers, or furniture.
- **Misjudging Vertical Connections:** Failing to understand how different floors are connected, *e.g.*, not recognizing that a staircase or elevator is required to change levels.
- **Direct Path Fallacy:** Heading in a straight-line towards the target without first identifying a feasible path, thereby ignoring the need to follow corridors, detour around obstacles, or use doorways.
- Overlooking Drop-offs: Proposing a path that would lead to falling from a significant height, such as walking

off a balcony or over a ledge.

Lack of Socio-Spatial Commonsense. This error refers to the agent's inability to grasp the implicit social norms and functional roles of different areas in public spaces, leading to potential failures as follows:

- Violating Traffic Norms: Jaywalking across a busy driveway or road instead of using a nearby crosswalk or pedestrian lane.
- Trespassing Restricted Zones: Attempting to cut through behind a retail counter, through a staff-only area, across a floor hazard warning sign (*e.g.*, "Wet Floor"), or through a private property shortcut.
- **Disregarding Spatial Etiquette:** Violating implicit social norms that govern public behavior, *i.e.*, actions that are physically possible but socially disruptive, such as interrupting a queue or invading personal space.
- **Ignoring Functional Layouts:** Violating explicit architectural constraints and intended circulation paths, *i.e.*, attempting to navigate through physical obstructions (like tables or seats) rather than designated aisles.
- Misusing Spaces: Proposing to walk through a decorative fountain or flowerbed, or using an emergency exit as a routine shortcut.

Additional qualitative examples for all five error types (two for *HOS* and three for *HPS*) are provided in Figures VIII and XII.

VIII. Case Study

In this section, we provide qualitative case studies (See Figs. XIII-XV) comparing the behavior of the model before and after post-training. For each case, we focus on one of the three key capabilities introduced by post-training, as described in Sec. 5.3.

Inference Prompt

SYSTEM PROMPT - HOS

You are a robot and perform object searching tasks according to instructions. Your goal is to rotate the camera to center the target object in the camera view, and then submit the task. The camera center is presented as a green cross in the picture.

SYSTEM PROMPT - HPS

You are a robot and perform navigation tasks according to instructions. Your goal is to turn your camera center to the target direction you need to move towards to reach the target location. The camera center is presented as a green cross in the picture. Don't move in the unavailable direction, such as obstacles or gaps.

Actions you can take: rotate(yaw:int,pitch:int), submit(yaw:int,pitch:int)

rotate(yaw:int,pitch:int): rotate the camera in the yaw and pitch direction relative to the current direction. Yaw is the rotation angle in the x-y plane, pitch is the rotation angle in the y-z plane. Yaw angle < 0 means rotate to the right, yaw angle < 0 means rotate to the left. Pitch angle > 0 means look up, pitch angle < 0 means look down.

submit(yaw:int,pitch:int): submit the task with the current camera view with the target object at the center, yaw and pitch are the angles of the current camera view, which is reported by the environment. You can only take one action at a time. The instruction will be provided with each observation. Look at the image carefully to complete the instruction.

FEW SHOT EXAMPLE (disabled after training)

Example:

Round 1: image_1

<think>I need to find the coffee machine. I can see a table on on my left, a couch in front of me, and a door to the right. The coffee machine is likely on the table, which is to my left.

Round 2: Env_feedback: Last action is executed successfully, your current direction (yaw,pitch) is (315,0).

image_2

<think>From the secene, I see that by turning left 45 degrees, a kitchen table is in front of me. The coffee machine is on the left of the table and slightly lower than the camera center. I need to turn leftward and downward a little bit.
kitchen table is in front of me. The coffee machine is on the left of the table and slightly lower than the camera center. I need to turn leftward and downward a little bit.

Round 3: Env_feedback: Last action is executed successfully, your current direction (yaw,pitch) is (285,-5).

image_3

<think>The coffee machine is right now at the center of my camera, I think I can submit the task.</think> <answer>submit(285,-5)</answer>

Round 4: Env_feedback: Success

You can take 1 action(s) at a time. You should first give your thought process, and then your answer.

Your response should be in the format of: <think>...</think><answer>...</answer>

e.g. <think>I need to find the coffee machine. I can see a table on on my left, a couch in front of me, and a door to the right. The coffee machine is likely on the table, which is to my left.</think><answer>rotate(-45,0)</answer>

USER PROMPT

After your answer, the extracted valid action is {valid_action}.

The environment feedback is: {env_feedback}

done: {done}

After that, the observation is: {observation}

Human Instruction: {instruction}

Decide your next action.

You can take 1 action(s) at a time. You should first give your thought process, and then your answer.

Your response should be in the format of: <think>...</think><answer>...</answer>

Figure II. Prompt used for inference and rollout.

Examples of **HOS** Tasks

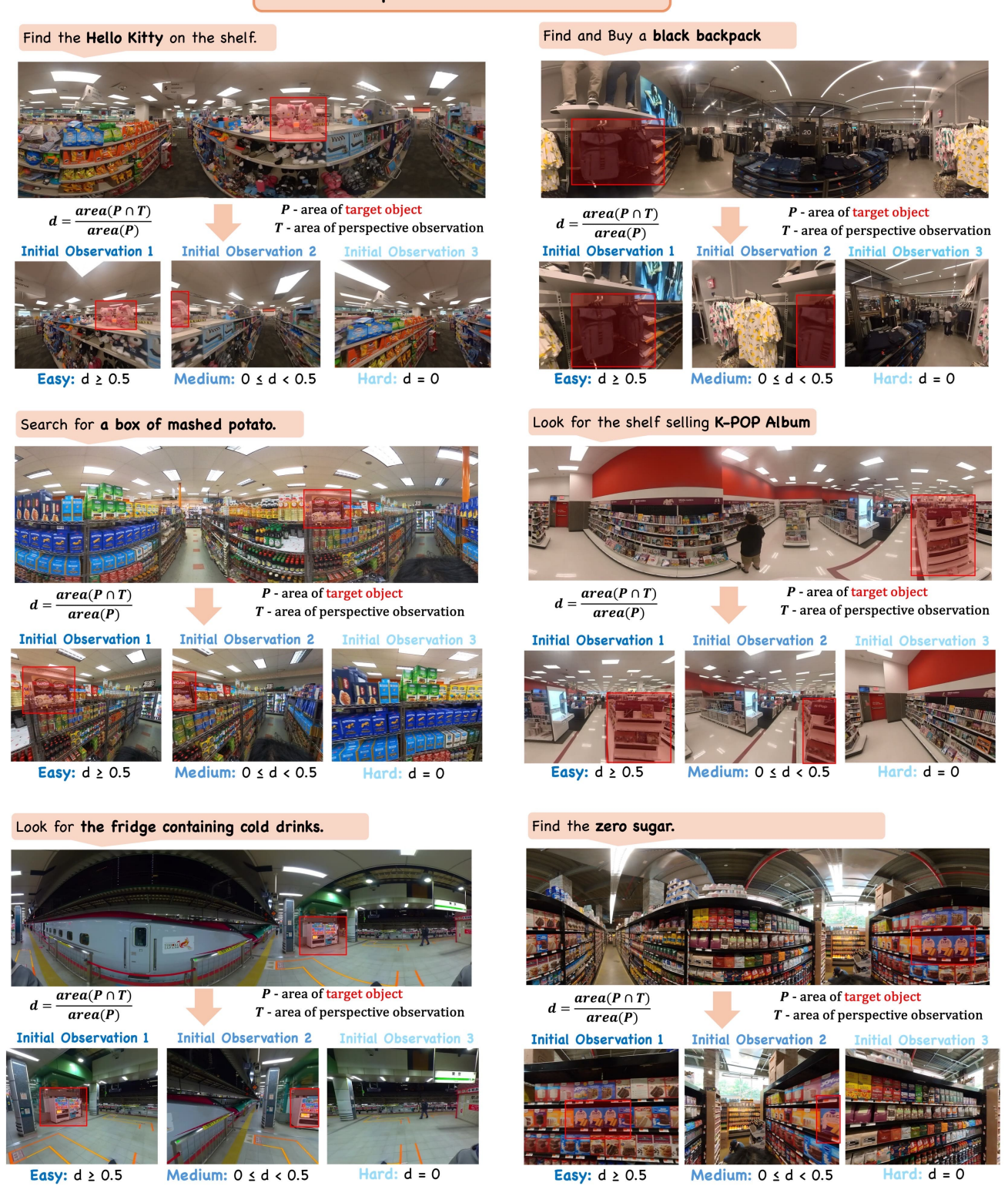


Figure III. Visualizations of *HOS* task instances.

Easy-Level Examples of HPS Tasks

Easy-level Task: You want to go into a store EYEWORLD OPTICAL, which direction are you going to move?





Aligned directions of Cue and Motion with textual instruction.

Direction of Motion



Direction of Cue

Easy-level Task: You want to go to 9th Avenue, which direction are you going to move?





Aligned directions of Cue and Motion with textual instruction.



Direction of Motion



Direction of Cue

Easy-level Task: You want to exit this platform, which direction are you going to move?







Aligned directions of Cue and Motion with textual instruction.

Direction of Motion

Easy-level Task: You want to buy some jewelry, which direction are you going to move?





Aligned directions of Cue



Direction of Motion and Motion with textual

Direction of Cue

Easy-level Task: You want to take the subway line 4, which direction are you going to move?



Easy-level Task: You want to enter the building called ONE FIVE ONE, which direction are you going to move?



Aligned directions of Cue and Motion with textual instruction.



Direction of Motion



Direction of Cue





Aligned directions of Cue and Motion with textual instruction.



Direction of Motion



Direction of Cue

Figure IV. Visualizations of easy-level HPS task instances.

Medium-Level Examples of HPS Tasks

Medium-level Task: You want to exit, which direction are you





Misaligned directions of Cue and Motion with textual instruction.

Direction of Motion Direction of Cue

Medium-level Task: You want to go to Gate E, which direction are you going to move?





Misaligned directions of Cue and Motion with textual instruction.

Direction of Cue

Medium-level Task: You want to go to Fulton Center, which direction are you going to move?





Misaligned directions of Cue and Motion with textual instruction.

Direction of Motion

Medium-level Task: You want to play PHOENIX Roller Coaster, which direction are you going to move?





Misaligned directions of Cue and Motion with textual instruction.

Direction of Motion



Medium-level Task: You want to go Room 104, which direction are you going to move?





Misaligned directions of Cue and Motion with textual instruction.



Direction of Motion



Direction of Cue

Medium-level Task: You want to take the subway to the brooklyn, which direction are you going to move?





Misaligned directions of Cue and Motion with textual instruction.



Direction of Motion



Direction of Cue

Figure V. Visualizations of medium-level HPS task instances.

Hard-Level Examples of HPS Tasks

Hard-level Task: You need to leave this airport, which direction are you going to move?





Aligned directions of Cue and Motion without textual instruction.



Direction of Motion



Direction of Cue

Hard-level Task: You want to take the stairs to the subway station, which direction are you going to move?









Aligned directions of Cue and Motion **without** textual instruction.

Direction of Motion

Direction of Cue

Hard-level Task: You want to take a taxi, which direction are you going to move?





Aligned directions of Cue and Motion **without** textual instruction.



Direction of Motion



Direction of Cue

Hard-level Task: You want to go into the shopping mall, which direction are you going to move?





Aligned directions of Cue and Motion **without** textual instruction.



Direction of Motion



Direction of Cue

Hard-level Task: You want to have a meeting with your teammates, which direction are you going to move?





Aligned directions of Cue and Motion **without** textual instruction.

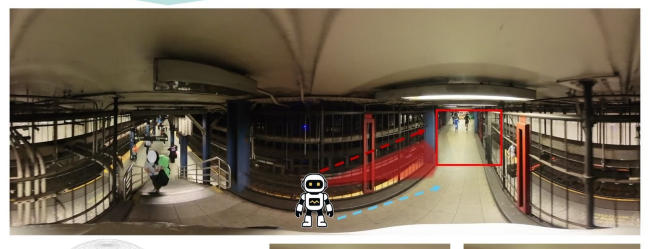


Direction of Motion



Direction of Cue

Hard-level Task: You want to leave this subway station, which direction are you going to move?





Aligned directions of Cue and Motion **without** textual instruction.



Direction of Motion



Direction of Cue

Figure VI. Visualizations of hard-level HPS task instances.

Extreme-Level Examples of HPS Tasks

Extreme-level Task: You need to leave this subway station, which direction are you going to move?





Misaligned directions of Cue and Motion without textual instruction.



Direction of Motion



Direction of Cue

Extreme-level Task: You would like to inquire about the price of the green sweaters on display, where are you going to move?





Misaligned directions of Cue Direction of Motion and Motion without textual instruction.



Direction of Cue

Extreme-level Task: You want to take escalator to go upstairs, which direction are you going to move?





Misaligned directions of Cue and Motion without textual instruction.



Direction of Motion



Direction of Cue

Extreme-level Task: You want to go to the opposite platform, which direction are you going to move?





Misaligned directions of Cue and Motion without textual



Direction of Motion



Direction of Cue

Extreme-level Task: You want to go the platform below, which direction are you going to move?





Misaligned directions of Cue and Motion without textual instruction.



Direction of Motion



Direction of Cue

Extreme-level Task: You want to have a seat, which direction are you going to move?





Misaligned directions of Cue and Motion without textual instruction.



Direction of Motion



Direction of Cue

Figure VII. Visualizations of extreme-level *HPS* task instances.

Q Limited Visual Grounding Capabilities



Figure VIII. Qualitative Examples of Limited Visual Grounding Capabilities in HOS.

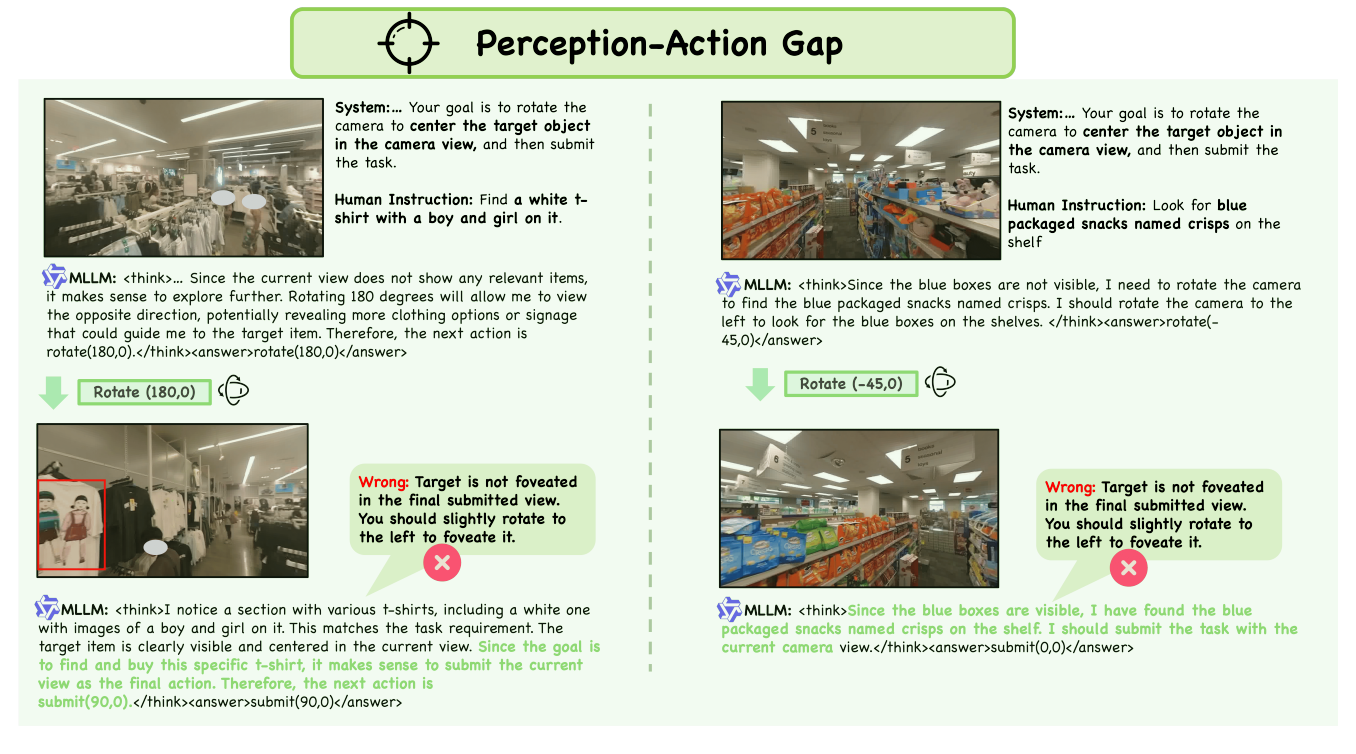


Figure IX. Qualitative Examples of Perception-Action Gap in HOS.

→ Vision-Action Mismatch



System: ... your goal is to rotate the camera to face the direction you need to move foward, and then submit the task.

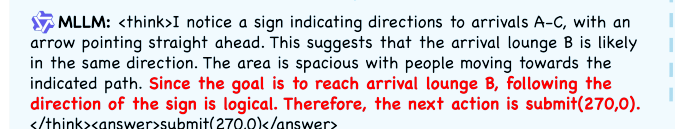
Human Instruction: you want to go to arrival lounge B, where are you going to move?

MLLM: <think>...Since there are no clear indicators for the arrival lounge B in this view, rotating 180° might reveal additional signage or pathways leading to the arrival lounge. Therefore, the next action is rotate(180,0). </think><answer>rotate(180,0)</answer>





Wrong: You should turn right to face the direction of arrival lounge B according to the sign.





System: ... your goal is to rotate the camera to face the direction you need to move foward, and then submit the task
Human Instruction: You want move to the direction of A C, where are

you going to move?

MLLM: <hi>MLLM: </p



Wrong: You should turn right to face the direction of the A&C according to the sign.



MLLM: <think>In the current image, the sign indicating the direction of the A and C lines is now directly in front of the camera center. This means the camera is aligned with the direction I need to move towards. I can now submit the task with the current direction.

Figure X. Qualitative Examples of Vision-Action Mismatch in HPS.

Lack of Physical Commonsense



System: ... Don't move in the unavailable direction, such as obstacles or gaps.

Human Instruction: You want to go to the opposite platform, where are you going to move?

MLLM: <think>The previous action rotated my camera to the right. Now I can see the other platform. I need to rotate my camera further to the right to move closer to the other platform. I should rotate my camera to the right a little bit more. <fthink><answer>rotate(45,0)</answer>





Wrong: You should first go upstairs to leave this platform, therefore you should continue to turn right to face the staircase.



System: ... Don't move in the unavailable direction, such as obstacles or gaps.

Human Instruction: You want to go downstairs, where are you going to

MLLM: <



Wrong: Your final submitted direction is not navigable, you should turn right to face the direction of staircase.

MLLM: <think>I can now clearly see the stairs. I need to submit the task now.</think><answer>submit(90,-30)</answer>

Figure XI. Qualitative Examples of Lack of Physical Commonsense in HPS.

Lack of Socio-Spatial Commonsense

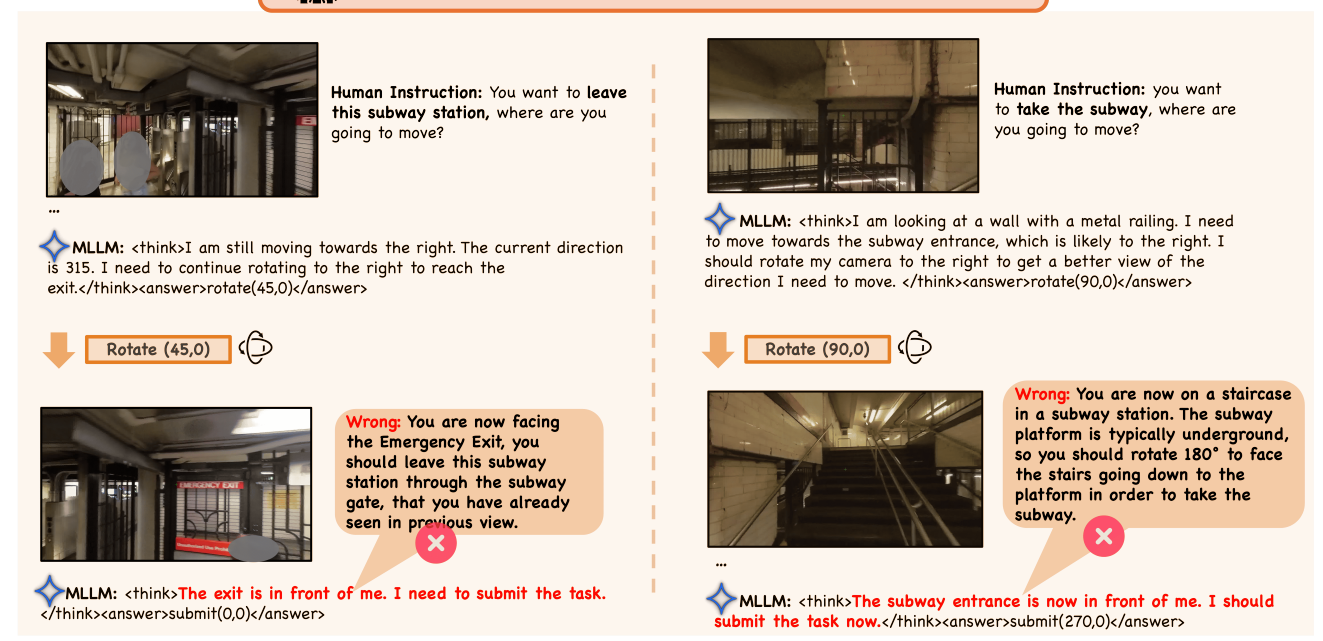


Figure XII. Qualitative Examples of Lack of Socio-Spatial Commonsense in HPS.

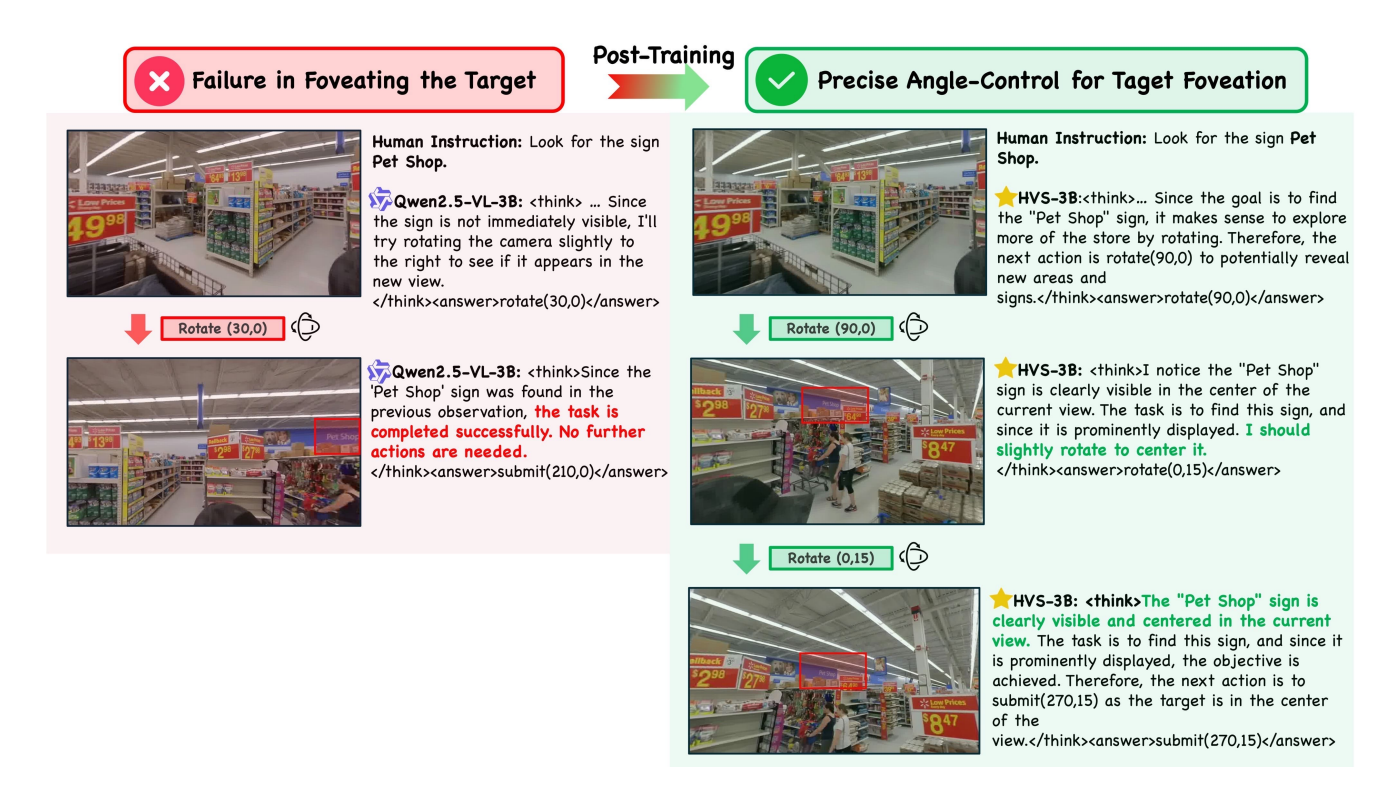


Figure XIII. Case study of target foveation. **Left**: Pre-trained model submits prematurely after coarse rotation toward "Pet Shop" sign, leaving target off-center. **Right**: Post-trained model performs corrective turn with fine-grained rotation to accurately center target before submission.

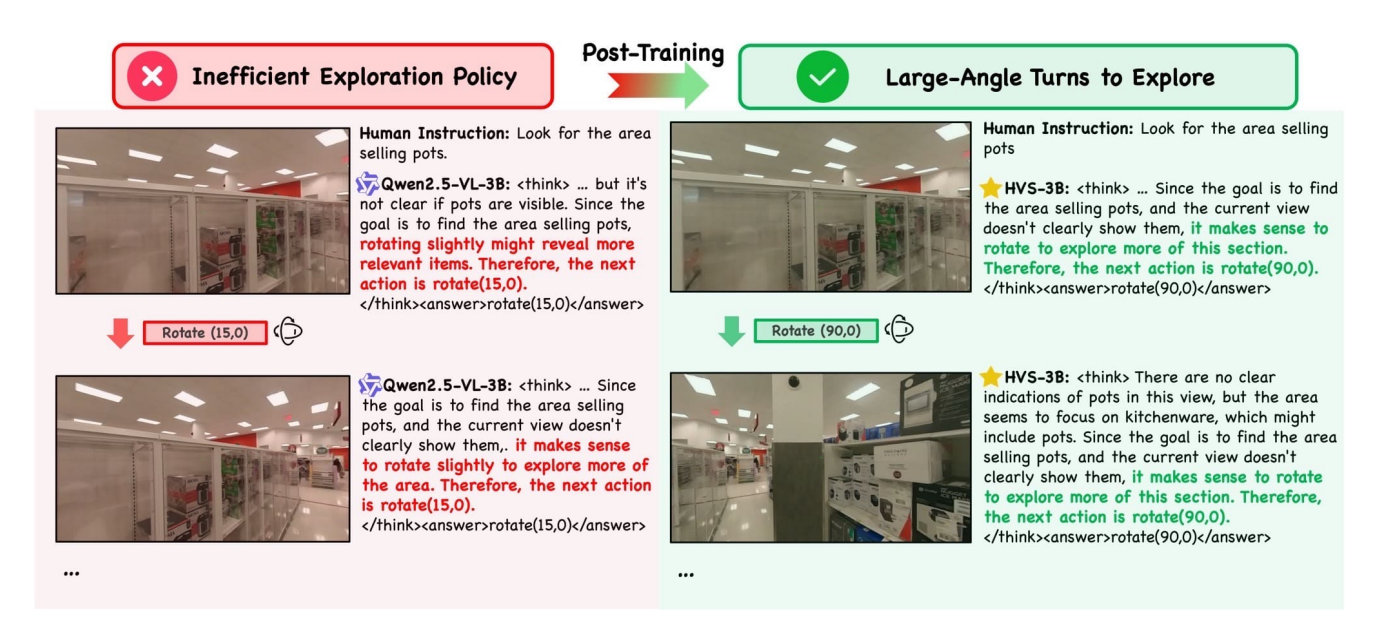


Figure XIV. Case study of exploration behavior. **Left**: The pre-trained model employs an inefficient exploration strategy, making repeated small-angle turns that provide little new information about the location of pots. **Right**: The post-trained model learns to perform large-angle exploratory turns, which quickly reveal new aisles and identify the target section, resulting in a more efficient search trajectory.

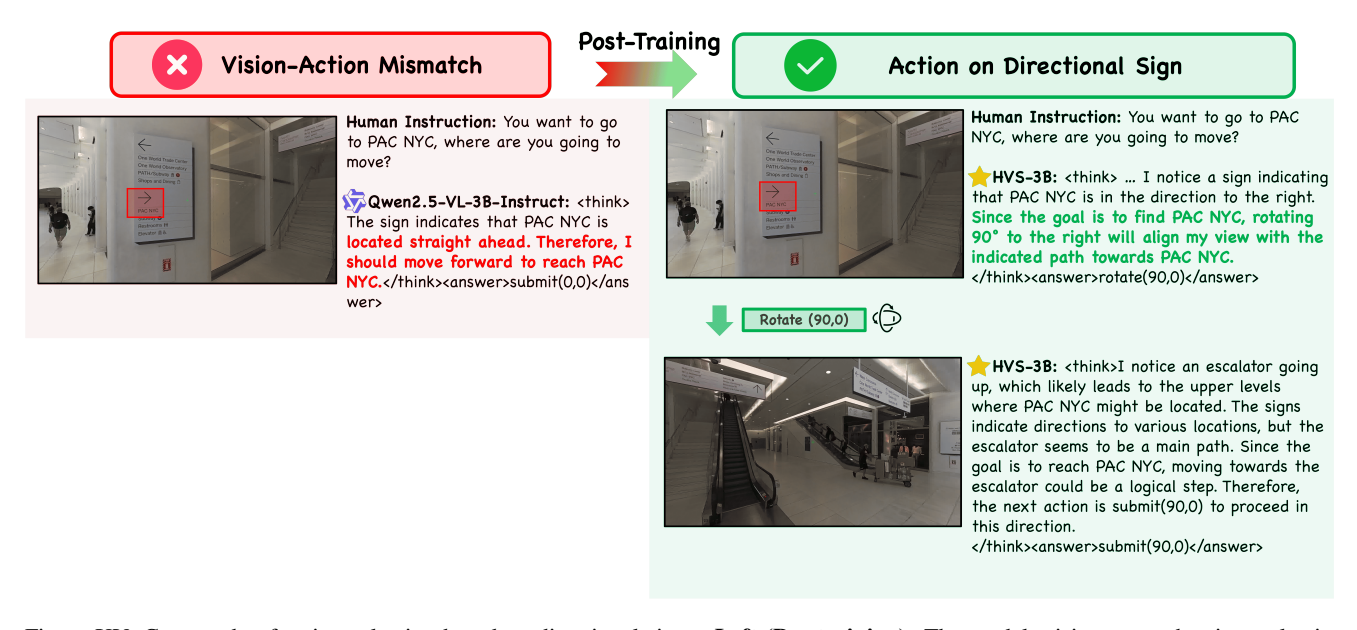


Figure XV. Case study of action selection based on directional signs. Left (Pre-training): The model misinterprets the sign, selecting an action that contradicts the indicated route and resulting in a vision–action mismatch. Right (Post-training): After training, the model correctly follows the sign's instruction, rotates 90° to align with the target direction, and proceeds towards the goal.